Determining homogeneity and amount of Calcium uptake in $Y_{1-\delta}Ca_{\delta}Ba_{2}Cu_{3}O_{7-x}$ crystals

W. Caiger
Level 3 MSci. Laboratory, School of Physics, University of Bristol.
(Dated: October 7, 2025)

Calcium doping of $Y_{1-\delta}Ca_{\delta}Ba_{2}Cu_{3}O_{7-x}$ (Ca-YBCO) is crucial the investigating the electron hole doping regime above that achievable by varying x alone. However, when reporting the superconducting properties of Ca-YBCO crystals often only the Calcium percentage added into the growth melt is given. Furthermore, there is no consideration of the homogeneity of Calcium uptake in the crystals. Scanning electron microscopy (SEM) is used to determine the actual Calcium uptake δ_c in six Ca-YBCO crystals from the same growth batch. It is shown that the distribution of Calcium within each crystal is homogeneous, however, there are fluctuations of δ_c between crystals of up to $1.97\% \pm 0.37$.

INTRODUCTION

One of the most widely researched ambient pressure high temperature superconducting compound is $Y_1Ba_2Cu_3O_{7-x}$ (referred to as YBCO). Variation of x from 1-0 changes the charge carrier density (p) by adding electron holes into the compound [1]. The relationship between p and superconducting properties is difficult to predict so must be obtained empirically [2]. However, the YBCO lattice consists of planes of CuO_2 , these become oxygen saturated, meaning without changing the crystal structure, the region of p above this level is only accessible by introducing holes at a different site. This has been done by replacing Y^{2+} ions with Ca^{3+} . The formula for Ca doped YBCO is then $Y_{1-\delta}Ca_{\delta}Ba_2Cu_3O_{7-x}$ (referred to as Ca-YBCO).

Growth of pure and homogeneous Ca-YBCO is difficult because of its high kinetic viscosity, low coefficient of diffusion [3] and incongruent melting characteristic [4], meaning it can only be grown in flux. Self-flux methods and more recently 'Top-seeded melt growth' solve these to a degree; promoting convection transport within the melt [3]. However, the uptake of Ca into the Y sites of the crystal is not 100% and is only assumed to be uniform. The issue presented by (2) is that under flux conditions many crucible materials become soluble, introducing defects into the crystal. Whilst this problem has been solved using Yttria-stabilised Zirconia crucibles [5], this material still imposes a limitation on the overall growth time of 100 hours before it too begins to corrode. This combined with the requirement for a slow growth rate seriously limits the size that crystals can reach without compromising purity.

The present issue is that in much of the literature on the effects of Ca doping on the superconducting properties of Ca-YBCO reference only the nominal Ca percentage added to the melt (δ_m) without consideration for the actual yield of Ca into the crystal structure (δ_c) . Furthermore, inhomogeneous O uptake [6] and stability are known problems depending strongly on growth conditions [7], yet little consideration of Ca distribution has been made (except of Ca at grain boundaries has been measured in Ca-YBCO films using High resolution Secondary Ion Mass Spectroscopy [8]). Therefore, the joint aims of this paper are to establish the degree to which Ca uptake in the crystal structure is homogeneous and to determine δ_c .

Electron beam microscopy has been used to measure the

oxygen content in pure YBCO crystals [9, 10]. Limitations to these experiments came from the small x-ray scattering cross section of O. This will present less of an issue when measuring Ca.

EXPERIMENTAL DETAILS

The scanning electron microscope (SEM) used for this experiment was the TESCAN VEGA3 fitted with apparatus for three different imaging modes; secondary electron (SE) imaging, backscattered electron (BSE) imaging and energy dispersive x-ray spectroscopy (EDS). Data from each of these modes was combined to identify and characterise defect sites and phases within six different Ca-YBCO crystals collected from the same growth batch. The growth process followed [11] using a Y-stabalised ZrO2 crucible and $\delta_m=15\%$.

The primary method of data collection was using EDS mode with Oxford Instruments Aztec software to create 2D maps of crystal composition at wide $(200\mu m)$, medium $(25\mu m)$ and zoomed $(3\mu m)$ scales on each crystal. For each crystal a map was taken first at wide scale, then areas of particular interest (exhibiting particularly homogeneous or inhomogeneous features) were chosen for medium scale maps, with the zoomed scale maps within those again. Most EDS data was collected with an electron beam voltage of HV = 30keVand beam intensity of 15.9 - 16.5 (arb. units), achieving optimal dead times of 58-60%. This beam voltage was necessary to capture high energy emissions of yttrium at $K_{\alpha 1} = 15 keV$ and $K_{\beta 1} = 16.9 keV$. Further investigation at lower HV =10keV was used to capture compositional information at a lower penetration depth, assuming isotropic decrease of the penetration volume with decreasing HV.

Firstly, our own python script was used to discern and quantify inhomogeneities in Ca distribution. All maps were processed to determine homogeneity at varying scales. Moran's I (M_I) was used to determine the degree of spatial correlation in a map. Spearman's rank (ρ_S) together with variogram analysis was used to quantify spatial cross-correlation between maps.

Secondly, quantitative compositional data was collected from Aztec's semi-standardless quantitative analysis tool [12]. The zoomed maps presented optimal conditions for quantitative EDS analysis [13], so $\bar{\delta}_c$ was calculated for each crystal using an average of data from multiple zoomed scans.

RESULTS and DISCUSSION

Calcium Homogeneity

Surface Phase Characterisation

Phases of increased Ca, C and O were identified from EDS maps. From investigating these phases at varying HV with a combination of EDS, SE and BSE data it was clear these corresponded to surface defects which were not related to the composition of the Ca-YBCO crystal below.

At HV = 30keV phases of high Ca corresponded to slight decreases in other Ba and Cu but almost no change in Y was observed. At lower HV = 10keV the same phases still corresponded to increases in Ca, C and O but now also to significant decreases in Ba, Cu and Y. Furthermore, SE images like Fig 1 of these regions showed a change in surface morphology between the surrounding flat crystal surface and these phases. Finally, taking images in BSE mode at low HV the regions exhibited a significant contrast – appearing darker, implying lower average atomic mass – to the surrounding area; whereas at high HV almost no contrast was observed. The stronger expression of phases at smaller penetration depths EDS and BSE data demonstrates the phases were near the surface of the crystal. The distinct change in surface morphology captured by the SE images is consistent with either the crystal structure being altered entirely, or simply defects on the surface of the Ca-YBCO.

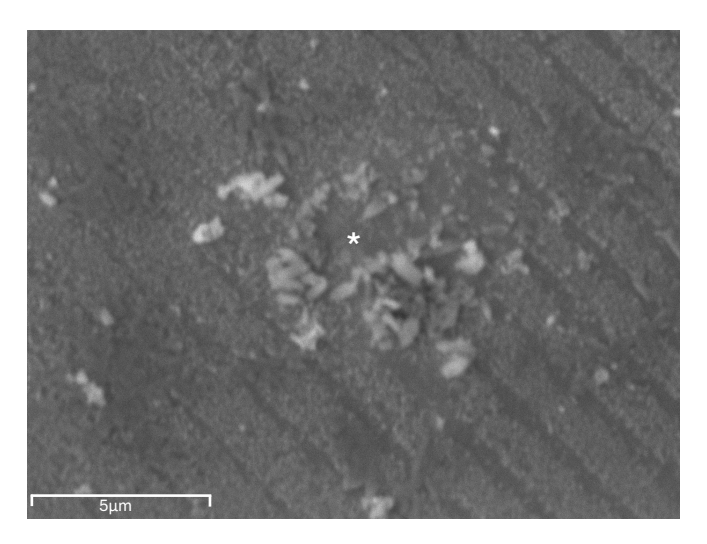


FIG. 1. shows an SE image of crystal D at medium scale where * is a example of a Ca, C and O phase identified using EDS.

These can be explained by the precursor for Ca in the melt mixture. CaCO₃ was used, strongly implying these areas corresponded to surface defects of CaCO₃ which did not properly integrate into the melt during crystal growth. This result of surface contamination is consistent with [14] where the surface is not representative of the bulk. Specific furnace programs have been altered to decompose carbonates [3].

Numerical Analysis of Visually Homogeneous Regions

Areas outside of these surface phases appeared homogeneous under visual inspection. On further statistical testing on

EDS map data of these areas, fluctuations in pixel brightness $(b_{i,j})$ of up to 8 standard deviations from the mean were found in Ca, Y, Ba, Cu and O. Though, the following tests of global Moran's I; variogram analysis; spatial cross-correlation; and variation under scale in parallel with the consistency of these measures between all elements suggests it is unlikely that high-brightness pixels correspond to actual inhomogeneities in the crystal composition.

From calculating the variation on the mean,

$$V_{i,j} = \bar{b} - b_{i,j} \tag{1}$$

for each pixel in the map array i,j it became clear the distribution of $V_{i,j}$ was asymmetric around zero. $V_{i,j}$ ranged from $-1 < V_{i,j} < 8$ in Ca, Y, Ba and Cu at all scales.

The data was filtered to obtain only the brightness values corresponding to significant fluctuations from the mean $V_{i,j}^*$, where setting n=3 is shown in Fig 2.

$$V_{i,j}^* \ge n\sigma_b. \tag{2}$$

In Fig 2 there are two visually identifiable Ca defect sites at positions A and B (where A corresponds to Fig 1). Outside of these defect sites it is difficult to tell if the distributions of Ca and Y significant fluctuations is random or structured in some way. Frequency plots of the number of standard deviations from the mean (n_{σ}) of each pixel were made and shown to have a strong fit with an exponential function. So, the number of pixels of a certain n_{σ} decayed roughly exponentially.

Next, to determine the spatial distribution of these infrequent high-brightness pixels two consequences of them corresponding to actual inhomogeneities are considered, and then shown to be counterfactual. Firstly, if we assume it is only possible for Ca to replace Y in the crystal structure (as opposed to Ba, Cu or O) there should be a negative (anti)correlation between the location of Ca and Y fluctuations. Secondly, the significant fluctuations would have a structured distribution at some scale, like clustering.

Condition (1) was tested by calculating a global spatial correlation coefficient between Ca and Y maps of the same scan using Spearman's rank. The value of ρ_S did not vary with the map scale. The range of ρ_S over all maps was -0.008 to 0.006. With this method the data from Fig 2 (bottom) gave $\rho_S = -0.090$, ordinary interpretation of this value would indicate an extremely weak anti-correlation, however, it clear from visual inspection that there is an anti-correlation. Even with this consideration, the values of ρ_S on homogeneous sites gave roughly as many negative as positive values, suggesting no global trend between Ca and Y distribution and that the data is truly uncorrelated.

Condition (2) was tested through calculating the global Moran's I coefficient (M_I) [15] on homogeneous subset of Ca and Y maps alongside variogram analysis.

$$M_{I} = \frac{\sum_{i} \sum_{j \neq i} w_{i,j} (b_{i} - \bar{b}) (b_{j} - \bar{b})}{\left(\frac{1}{N} \sum_{i} (b_{i} - \bar{b})^{2}\right) \sum_{i} \sum_{j \neq i} w_{i,j}}$$
(3)

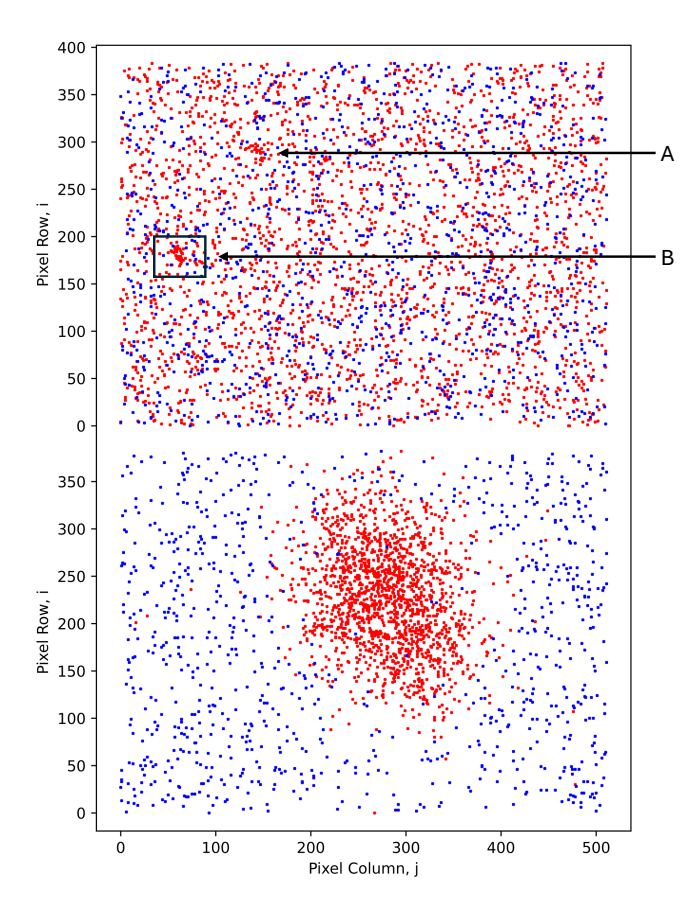


FIG. 2. Shows the maps of Ca (red) and Y (blue) overlaid for crystal F medium scale (left) and zoomed scale (right), which corresponds to area A. This is a schematic representation as the points are larger than the actual pixel size and the pixels are coloured or white in a binary response to Equ (2) for clarity.

where N is the number of pixels and using a first order queen contiguity spatial weight matrix $(w_{i,j})$, where correlation is weighted preferentially towards each pixels' nearest neighbour. M_I did not differ between scales and on average was $M_{I,Ca}=0.003$ for Ca and $M_{I,Y}=0.0004$ for Y maps, both values imply very little spatial correlation. One limitation to this calculation is the choice of $w_{i,j}$ [16], where correlation might be present on a larger scale e.g. between a pixel and its m^{th} nearest neighbour.

The variogram plots for scan containing a defect (1) and one without (2) are shown in Fig 3.

$$\gamma(h) = \frac{1}{N(h)} \sum_{i=1}^{n} \sum_{j=1}^{m} (x_{ij} - x_{i+h,j+h})^{2}$$
 (4)

where the semivariance $\gamma(h)$, is calculated by averaging the the variance between a pixel and all pixels of lag h away from it along n rows and m columns (with total number of pixels of each h=N(h)). The linear trend of Ca₁ suggests spatial correlation between pixels up to 100 pixels apart, whereas the flat gradient of Y₁, Ca₂ and Y₂ semivarience over the full range of spatial lags suggest no correlation on any scale.

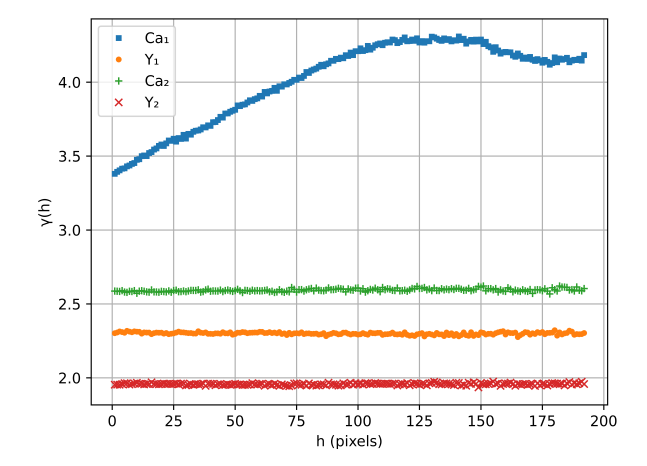


FIG. 3. Shows the plot of semivariance $(\gamma(h))$ against lag (h) for Ca and Y from a defect-containing medium scan and a visually homogeneous scan from crystal D.

Pertaining also to condition (2); if the high-brightness pixels in the wide scale maps correspond to actual inhomogeneities then one would expect the area corresponding to that pixel in the medium or zoomed scale maps to contain a cluster of adjacent high-brightness pixels. Clustering of this kind is not found in the data.

Since it can be assumed the distribution of Ba and Cu at the very least is consistent throughout the crystal else it would not grow, the fact that the character of $V_{i,j}^*$ in Ca and Y is also exhibited in Ba and Cu maps suggests such fluctuations should be discounted. This concludes the weight of evidence against the hypothesis that the fluctuation in $b_{i,j}$ in visually homogeneous regions.

Calcium Yield

The quantitative data extracted from the zoomed EDS maps gave values of $\bar{\delta_c}$ in the range of $1.97\% \pm 0.37$ with crystal A being an apparent anomaly at 22.12% as shown in Table .

Crucially, variation in $\bar{\delta_c}$ between crystals B-F was outside of the error, whilst the variation in δ_c between repeats within the same crystal remained comparably constant, for example the range over the repeats on crystal B was 0.1%.

TABLE I. Quantitative Ca data from averages over zoomed $(1\mu m)$ scale giving $\bar{\delta_c}$ where δ_R is the range of the averaged data set. $\bar{\delta_c}$ is used in conjunction with Fig 4 to predict T_c .

Crystal	$ar{\delta_c}(\%)$	$\delta_R(\%)$	$T_c(K)$
A	22.21 ± 0.21	1.9	83.16 ± 0.89
В	5.51 ± 0.18	0.1	90.70 ± 0.80
C	6.13 ± 0.16	1.5	90.42 ± 0.75
D	7.48 ± 0.19	0.1	89.80 ± 0.82
Е	7.48 ± 0.15	0.9	83.16 ± 0.71
F	6.40 ± 0.14	0.1	90.29 ± 0.67

Aztec's quantitative analysis process was found through empirical testing by Oxford Instruments to be correct to within 2.1% of the known value on 95% of tested compounds [12].

Propagating this error forwards to δ_c gave uncertainties in the range of $\pm 0.51-0.67$ and the errors after averaging over repeats can be seen in Table . In this propagation it is assumed that the compound we are measuring falls within the 95% of tested compounds. However, if it is not, then literature suggests an error of up to $\pm 25\%$ [17].

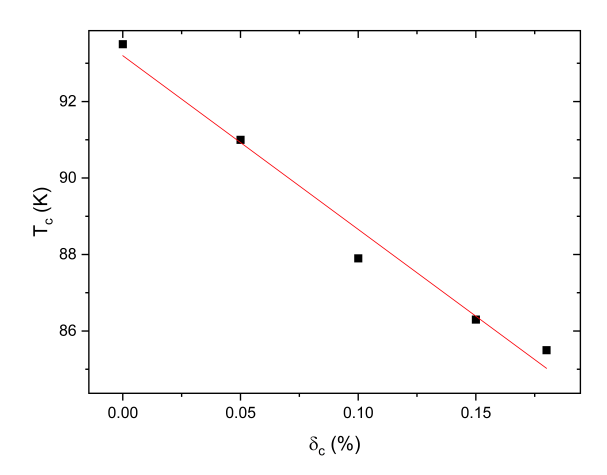


FIG. 4. Shows data of measured T_c and δ_c in Ca-YBCO crystals from 4 with a linear fit calculated. Note, there were no errors given with the data.

Making use of Bernhard and Tallon's data of T_c measured as a function of δ_c [18] an empirical fit was made in order to predict T_c for our crystals. This predicted value of T_c could be used to compare to measured T_c to verify the results of $\bar{\delta}_c$. In lieu of any other theoretical basis a linear fit was used as shown in FIG 4. Since $\bar{\delta}_c$ of crystal A was outside the range of the data from [18], our calculation of T_c is not reliable and thus $\bar{\delta}_c$ may not be verifiable b this method. Unfortunately, the data did not have errors associated with it. The error on T_c was propagated using the fit parameters standard errors calculated using Origin; which with very few relevant data points were large. As a result, the variation of predicted T_c between crystals fell within the range of the uncertainty on each value.

CONCLUSIONS

On the first aim to assess the homogeneity of Ca uptake in Ca-YBCO crystals, it has been shown the growth process contributes to notable surface defects. Whilst the internal crystal structure remains homogeneous under the test carried out here, the exact uptake of Ca varies between crystals grown in the same batch. The second aim to determine δ_c has been achieved up to the degree of confidence placed in the semistandardless EDS analysis approach used. More concrete evidence for the fluctuations of δ_c on the order of 1-2% can be achieved with further analysis using calibration standards.

Bibliography

[1] Y. Tokura, J. B. Torrance, T. C. Huang, and A. I. Nazzal, "Broader perspective on the high-temperature superconducting Yba₂cu₃o_y system: The real role of the oxygen content," *Phys. Rev. B*, vol. 38, pp. 7156–7159, Oct 1988.

- [2] R. Liang, D. Bonn, and W. Hardy, "Evaluation of cuo 2 plane hole doping in yba 2 cu 3 o 6+ x single crystals," *Physical Review B*, vol. 73, no. 18, p. 180505, 2006.
- [3] C. Lin, B. Liang, and H. Chen, "Top-seeded solution growth of ca-doped ybco single crystals," *Journal of Crystal Growth*, vol. 237-239, pp. 778–782, 2002. The thirteenth international conference on Crystal Growth in conj unction with the eleventh international conference on Vapor Growth and Epitaxy.
- [4] L. Schneemeyer, J. Waszczak, T. Siegrist, et al., "Superconductivity in yba2cu3o7 single crystals," Nature, vol. 328, no. 6131, pp. 601–603, 1987.
- [5] R. Liang, P. Dosanjh, D. Bonn, D. Baar, J. Carolan, and W. Hardy, "Growth and properties of superconducting ybco single crystals," *Physica C: Superconductivity*, vol. 195, no. 1, pp. 51–58, 1992.
- [6] C. Chen, "The microstructure of high-temperature oxide superconductors," *Physical Properties ofHigh Temperature Supre*conductors, edited by DM Ginsberg (World Scientific, Singapore, 1994), vol. 2, p. 199, 1990.
- [7] J. D. Jorgensen, B. W. Veal, W. K. Kwok, G. W. Crabtree, A. Umezawa, L. J. Nowicki, and A. P. Paulikas, "Structural and superconducting properties of orthorhombic and tetragonal Yba₂cu₃o_{7-x}: The effect of oxygen stoichiometry and ordering on superconductivity," *Phys. Rev. B*, vol. 36, pp. 5731–5734, Oct 1987.
- [8] C. Dark, M. Kilburn, G. Hammerl, C. Schneider, J. Mannhart, and C. Grovenor, "Nanosims analysis of ca doping at a grain boundary in a superconducting ybco ca-123/123 bicrystal," in *Journal of Physics: Conference Series*, vol. 43, p. 272, IOP Publishing, 2006.
- [9] J. T. Armstrong, "Determination of chemical valence state by x-ray emission analysis using electron beam instruments: Pitfalls and promises," *Analytical Chemistry*, vol. 71, no. 14, pp. 2714–2724, 1999.
- [10] K. L. Keester, R. M. Housley, and D. B. Marshall, "Growth and characterization of large yba2cu3o7x single crystals," *Journal* of Crystal Growth, vol. 91, no. 3, pp. 295–301, 1988.
- [11] D. M. Ginsberg, Physical Properties of High Temperature Superconductors III. WORLD SCIENTIFIC, 1992.
- [12] Oxford Instruments NanoAnalysis, "What is standardless quantitative analysis?."
- [13] Dartmouth College, "Introduction to eds analysis."
- [14] D. Werder, C. Chen, M. Gurvitch, B. Miller, L. Schneemeyer, and J. Waszczak, "Ba2ycu3o7 crystal surface layers: Orthorhombic splitting, dislocations, and chemical etching," *Physica C: Superconductivity*, vol. 160, no. 5, pp. 411–416, 1989.
- [15] X. Zhou and H. Lin, *Moran's I*, pp. 725–725. Boston, MA: Springer US, 2008.
- [16] K. Suryowati, R. Bekti, and A. Faradila, "A comparison of weights matrices on computation of dengue spatial autocorrelation," in *IOP Conference Series: Materials Science and En*gineering, vol. 335, p. 012052, IOP Publishing, 2018.
- [17] J. I. Goldstein, D. E. Newbury, J. R. Michael, N. W. Ritchie, J. H. J. Scott, and D. C. Joy, Scanning electron microscopy and X-ray microanalysis. springer, 2017.
- [18] C. Bernhard and J. L. Tallon, "Thermoelectric power of $y_{1-x}ca_xba_2cu_3o_{7-\delta}$: Contributions from cuo_2 planes and cuo chains," *Phys. Rev. B*, vol. 54, pp. 10201–10209, Oct 1996.